

Article

Tetranuclear Hetero-Metal $[\text{Mn}^{\text{III}}_2\text{Ni}^{\text{II}}_2]$ Complexes Involving Defective Double-Cubane Structure: Synthesis, Crystal Structures, and Magnetic Properties

Yuki Suemitsu ¹, Ryuji Matsunaga ¹, Takashi Toyofuku ¹, Yasunori Yamada ¹, Masahiro Mikuriya ² , Tadashi Tokii ¹ and Masayuki Koikawa ^{1,*} 

¹ Department of Chemistry and Applied Chemistry, Faculty of Science and Engineering, Saga University, Honjo 1, Saga 840-8502, Japan; 17574011@edu.cc.saga-u.ac.jp (Y.S.); 07538017@koi-ken.info (R.M.); toyofuku@koi-ken.info (T.T.); yyamada@cc.saga-u.ac.jp (Y.Y.); tokiit@cc.saga-u.ac.jp (T.T.)

² Department of Applied Chemistry for Environment, School of Science and Technology, Kwansei Gakuin University, Gakuen 2-1, Sanda 669-1337, Japan; junpei@kwansei.ac.jp

* Correspondence: koikawa@cc.saga-u.ac.jp; Tel.: +81-952-28-8549

Received: 29 December 2018; Accepted: 8 February 2019; Published: 14 February 2019



Abstract: Tetranuclear hetero-metal $\text{Mn}^{\text{III}}_2\text{Ni}^{\text{II}}_2$ complexes, $[\text{Mn}_2\text{Ni}_2(\text{L})_4(\text{OAc})_2]$ (**1**) and $[\text{Mn}_2\text{Ni}_2(\text{L})_4(\text{NO}_3)_2]$ (**2**) [$\text{H}_2\text{L} = N$ -(2-hydroxymethylphenyl)-5,6-benzosalicylideneimine], have been synthesized and characterized by X-ray crystal structure analyses, infrared spectra, and elemental analyses. The structure analyses revealed that the complexes have a defective double-cubane metal core connected by μ_3 -alkoxo bridges. Complexes consist of two bis- μ -alkoxo bridged $\text{Mn}^{\text{III}}\text{Ni}^{\text{II}}$ heteronuclear units making a dimer-of-dimers structure. The double-cubane cores are significantly distorted due to an effect of *syn-syn* mode acetato or nitrato bridges. Magnetic measurements indicate that weak antiferromagnetic interactions ($\text{Mn-Ni} = -0.66 \sim -4.19 \text{ cm}^{-1}$) are dominant in the hetero-metal core.

Keywords: tetranuclear complex; hetero-metal complex; manganese; nickel; crystal structure; double-cubane; Schiff-base ligand; magnetic property

1. Introduction

Molecular magnetism of discrete complexes with a cubane-based metal core structure have been extensively studied over the past few decades [1–4]. The key focal points of the investigation on such molecular magnetism are the following: (i) understanding of the basic correlation of spin coupling and molecular structure based on the analyses of the concerned orbitals [5]; (ii) application of the correlations in polynuclear systems that have several exchange pathways [6–8]; (iii) development of magnetic materials that behave like single molecule magnets (SMMs) [1–4,9]. In the case of tetranuclear complexes, two types of cubane-based structures are well known: cubane and double-cubane structures. The cubane core structures are commonly obtained with homo-metal complexes, whereas double-cubane structures are often formed by hetero-metal or mixed-valence complexes. This is due to the difference of the coordination environments between the metal ions located on the diagonal positions and those on the central positions, in the double-cubane structure. The hetero-metal complexes that form such double-cubane structures are a very interesting research target because they can be expected the synergy of hetero-metal ions, which may show unusual properties, such as selective catalytic ability or a ferromagnetic ground state. The *ONO*-tridentate ligands are well-known as good ligands for assisting the formation of cubane-like structures, as a result of the ability of their terminal

oxygen atoms to act as good bridging groups [10,11]. The tridentate Schiff base ligands obtained by a simple dehydration-condensation of salicylaldehyde and an aminoalcohol or aminophenol are useful for the preparation of cubane-based complexes [12,13]. In our previous research, we have reported that the Schiff base tridentate ligand, *N*-(2-hydroxymethylphenyl) salicylideneimine (H_2L1-H) [14] and its derivatives, can be used to produce cubane-like tetranuclear complexes via simple one-pot reactions [15–17]. As expected, these ligands gave hetero-metal or mixed-valence complexes characterized by a double-cubane metal core structure with a large high-spin ground state; such complexes included, for instance, $Mn^{III}_2Ni^{II}_2$ ($S_T = 6$) and $Co^{III}_2Co^{II}_2$ ($S_T = 3$) systems [16,17]. During our research work aimed at obtaining hetero-metal complexes, we found that the similar Schiff-base ligand *N*-(2-hydroxymethylphenyl)-5,6-benzosalicylideneimine (H_2L) produced novel $Mn^{III}Ni^{II}$ complexes comprising *syn-syn* bridging co-ligands as shown in Figure 1. We report here the syntheses, structures and magnetic properties of tetranuclear hetero-metal $Mn^{III}_2Ni^{II}_2$ complexes.

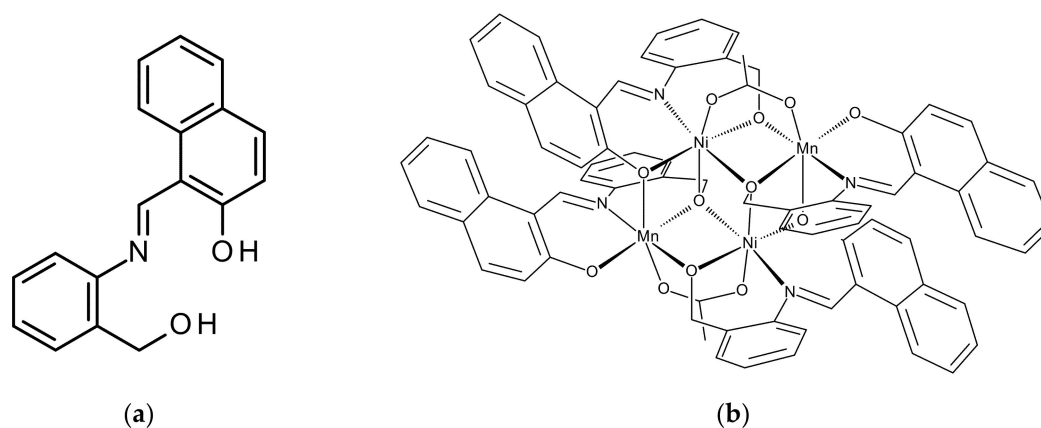


Figure 1. Chemical diagram of (a) ligand H_2L and (b) $[MnNi(L)_2(OAc)_2]$ (**1**).

2. Results and Discussion

2.1. Synthesis and Characterization of $[Mn_2Ni_2(L)_4(OAc)_2] \cdot H_2O$ (**1**) and $[Mn_2Ni_2(L)_4(NO_3)_2] \cdot 2H_2O$ (**2**)

Analytical data of the obtained complexes **1** and **2** gave 1:1:2:1 ratio of Mn, Ni, $(L)^{2-}$ ligand, and acetate/nitrate. In the infrared spectra (Figure S1 and Figure S2), these complexes show intense characteristic peaks at 1615 and 1619 cm^{-1} . These peaks can be assigned $\nu(C=N)$ vibration which shifted from free ligand H_2L (1620 cm^{-1}). A symmetric vibration (ν_{sym}) and an asymmetric vibration (ν_{asym}) of the *syn-syn* bridging acetate were observed at 1456 and 1582 cm^{-1} in the spectrum of **1**. For **2**, corresponding two signals of bridging nitrate were observed at 1456 and 1575 cm^{-1} .

2.2. Single Crystal X-ray Diffraction

Single-crystal X-ray diffraction measurements for **1** and **2** were performed at 293 K. The crystallographic data are summarized in Table S1. A molecular structure of **1** is shown in Figure 2 with atom numbering scheme. Additionally, selected bond distances and angles are summarized in Table 1 and Table S2.

The obtained crystals of **1** were unstable and efflorescence due to the large voids with highly volatile dichloromethane molecules. Many solvent systems were tested for recrystallization, but our attempts were in vain. All measurements were terminated by the cracking of the single crystals. Though the analytical results are insufficient to make a crystallographically accurate discussion, they clearly reveal the molecular structures to confirm the geometries of metal ions. As shown in Figure 2a, **1** has a tetranuclear structure with an inversion center. The final refined structural model of **1** is characterized by an asymmetric unit containing a Mn(III) ion and a Ni(II) ion, two $(L)^{2-}$ ligands, and one acetate anion. The Mn and Ni ions in the asymmetric unit of **1** rest on a dinuclear plane defined by a $[MnNi(L)_2]$ unit with bis- μ -alkoxo bridges from two deprotonated tridentate $(L)^{2-}$ ligands. Furthermore, an acetate anion is also present that act as *syn-syn* bridging

ligand coordinating the hetero-metals (Mn and Ni) at their axial positions. The symmetrically-related dinuclear units are linked to each other by two μ_3 -alkoxo (O1 and O1*) and two μ_2 -phenoxo (O4 and O4*) bridging atoms. Consequently, the tetranuclear hetero-metal core in **1** is best represented as a dimer-of-dimers. The metal atoms arrangement with bridging oxygen atoms in **1** can be viewed as the distorted defective double-cubane core structure. The valence states of the metal ions are confirmed by charge balance considerations, bond valence sum (BVS) calculations [18], and observations of Jahn-Teller elongations. The calculated BVS values are 3.25 and 2.22 for the Mn(III) and Ni(II) ions, respectively [19]. The coordination environment of Mn1 is a distorted octahedral geometry in which the equatorial positions are occupied by three oxygen atoms (O1, O2, and O3) and one nitrogen (N1) atom, whereas the axial positions are occupied by two oxygen atoms (O4* and O5). The bond distances in the equatorial plane of Mn1 are in 1.882(8)–1.981(9) Å range. The axial bond distances [2.135(7) and 2.410(7) Å] are longer than their counterparts in the equatorial plane, due to Jahn-Teller distortions that are typical for Mn(III) ions. The coordination geometry of Ni1 is also octahedral. The combination of atoms coordinating Ni1 is the same as that coordinating Mn1. However, the deviation of coordination bond distances [1.986(7)–2.141(7) Å] of Ni1 is within 0.155 Å, a substantially smaller value than in the case of Mn1. These distances are in the normal ranges for Mn(III) and Ni(II) complexes with Schiff-base ligands [16,20]. The *syn-syn* bridging acetate forces the structure to be folded with the value of the bent angle of the Mn(μ -O₂)Ni bridging fragment being equal to 15.8(2)°. The intramolecular metal-to-metal distances between Mn1...Ni1, Mn1...Ni1*, Ni1...Ni1*, and Mn1...Mn1* are 2.928(2), 3.255(2), 3.253(2), and 5.286(3) Å, respectively. The bond angles subtended by the μ_3 -alkoxo are 91.5(3)° for Mn1–O1–Ni1, 106.1(3)° for Mn1–O1–Ni1*, and 99.3(3)° for Ni1–O1–Ni1*. The short Mn1...Ni1 distance and narrow Mn1–O1–Ni1 angle is a common feature of *syn-syn* carboxylato bridging dinuclear structures [21]. The interdimer Mn1...Ni1* is much longer than the intradimer Mn1...Ni1 counterpart; additionally the bond angles Mn1–O1–Ni1* and Ni1–O1–Ni1* are much larger than 90°. Hence, the defective double-cubane core of **1** is highly distorted in the rhombic direction. Notably, the distorted core structure might be stabilized by intramolecular π – π stacking interactions as shown in Figure 2b [C9...C36* = 3.197(15), C11...C28* = 3.565(18), C13...C32* = 3.88(2), and C15...C34* = 3.621(17) Å, (*), (–x + 1, –y, –z)] between naphthyl groups belonging to the two asymmetric dimer units.

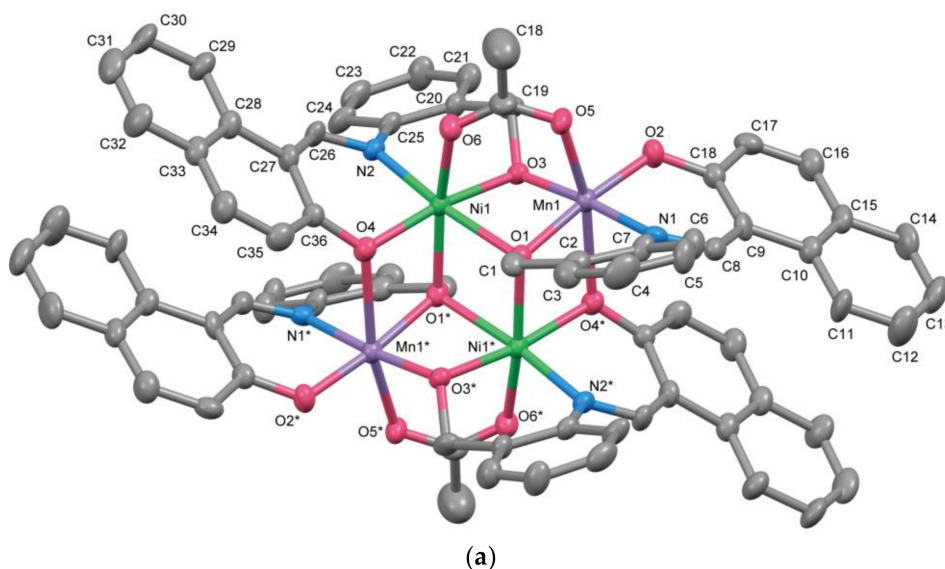


Figure 2. Cont.

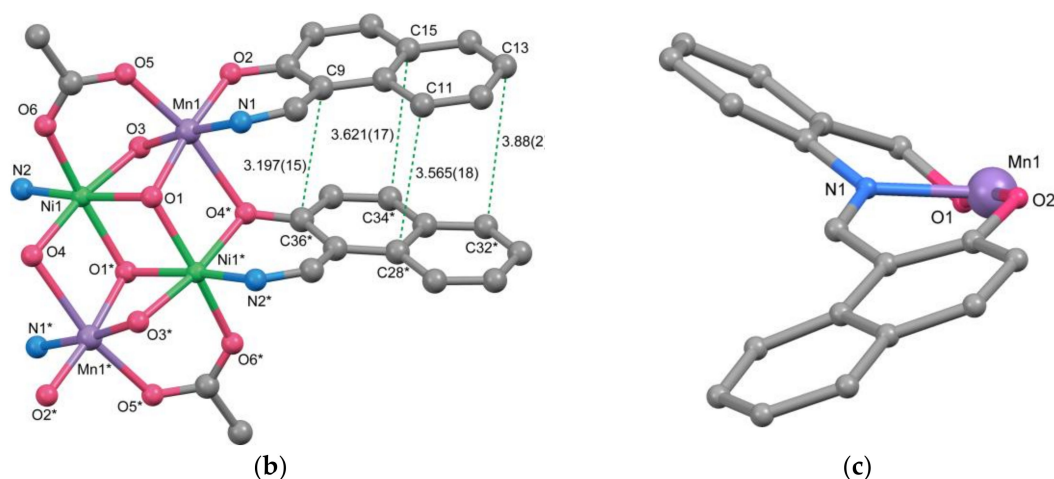


Figure 2. Crystal structure of **1**. (a) molecular structure, (b) modeling view for the intramolecular π - π stacking between naphthyl groups, (c) modeling view for the distortion of $(L)^{2-}$ in coordination. Thermal ellipsoids of (a) are drawn with 50% probability, hydrogen atoms are omitted for clarity. Symmetry code: (*) $-x + 1, -y, -z$.

Table 1. Selected bond lengths and angles of **1**, **2A**, and **2B**.

Bond/Angle	1 (Å)/(°)	2A (Å)/(°)	2B (Å)/(°)
Mn1–O1	1.943(7)	1.956(5)	1.938(5)
Mn1–O2	1.882(8)	1.874(5)	1.871(5)
Mn1–O3	1.907(6)	1.897(6)	1.924(7)
Mn1–O4 *	2.410(7)	2.331(6)	2.250(6)
Mn1–O5	2.135(7)	2.244(6)	2.261(6)
Mn1–N1	1.981(9)	1.980(7)	1.985(8)
Ni1–O1	2.141(7)	2.109(6)	2.117(6)
Ni1–O1 *	2.127(6)	2.107(6)	2.111(5)
Ni1–O3 *	2.005(7)	1.999(5)	1.987(5)
Ni1–O4 *	1.986(7)	1.977(5)	1.976(5)
Ni1–O6 *	2.077(7)	2.129(6)	2.156(5)
Ni1–N2 *	2.028(8)	2.012(7)	1.996(8)
Mn1...Ni1	2.928(2)	2.939(2)	2.952(2)
Mn1...Ni1 *	3.255(2)	3.193(2)	3.182(2)
Mn1...Mn1 *	5.268(3)	5.248(3)	5.244(3)
Ni1...Ni1 *	3.253(2)	3.183(3)	3.192(2)
Mn1–O1–Ni1	91.5(3)	92.5(2)	93.3(2)
Mn1–O1–Ni1 *	106.1(3)	103.6(2)	103.5(2)
Ni1–O1–Ni1 *	99.3(3)	98.0(2)	98.0(2)
Mn1–O3–Ni1	96.9(3)	97.9(3)	98.0(3)
Ni1–O4–Mn1 *	95.0(3)	95.3(2)	97.5(2)

Symmetry code (*): $-x + 1, -y, -z$ (**1**); $-x + 2, -y, -z + 1$ (**2A**); $-x + 2, -y + 1, -z + 2$ (**2B**).

The molecular structure of **1** resembles quite closely the structure of $[\text{Mn}_2\text{Ni}_2(\text{L1-H})_4(\text{OAc})_2]$ [$\text{H}_2\text{L1-H} = N$ -(2-hydroxymethylphenyl)salicylideneimine] [22]. In our previously reported complexes with L1-H ligand, the planarity of the ligand was considerably low because of the strain due to two adjacent 6-membered chelate rings [15–17,22]. For the present complex **1**, the deprotonated ligand $(L)^{2-}$ is also distorted at the imino group connecting the benzyl and naphthyl groups as shown in Figure 2c. The torsion angle of the C=N bond (C7–N1–C8–C9) is $164.6(8)^\circ$. The C–N bond of the aminobenzyl moiety is twisted, giving rise to a large dihedral angle [$50.1(3)^\circ$] between the phenyl and naphthyl groups. Due to such distortions and stacking interactions, the complex assumes a chair conformation like $[\text{Mn}_2\text{Ni}_2(\text{L1-H})_4(\text{OAc})_2]$. The crystal packing diagram of **1** is shown

in Figure S3. Notably, the structural features of the complex indicate that there is no remarkable intermolecular interaction.

The crystal structure of **2** comprises two crystallographically independent molecules. These two molecules (**2A** and **2B**) are shown in Figure 3, and selected bond distances and angles are summarized in Table 1. Each molecule in **2** has a similar tetranuclear structure with an inversion center. These complexes are comprised of two Mn and Ni ions, four (L)^{2−} ligands, and two nitrate anions (instead of the acetate anions present in **1**). The difference between **2A** and **2B** is the intramolecular π – π stacking between the naphthyl groups of H₂L in each molecule. The molecular structure of **2A** is almost the same as that of **1**. The small dihedral angle 5.0(2)° of naphthyl groups suggests the existence of a π – π stacking interaction in **2A**. The C···C distance between stacking naphthyl groups are C9A···C36A' = 3.145(12), C11A···C28A' = 3.249(12), C13A···C32A' = 3.457(13), and C15A···C34A' = 3.367(12) Å [(') $-x + 2, -y, -z + 1$], respectively. On the other hand, the corresponding dihedral angle in **2B** is very large [24.2(2)°] and the C···C distance between naphthyl groups are too distant [C9B···C36B'' = 3.277(11), C11B···C28B'' = 3.969(12), C13B···C32B'' = 4.871(13), and C15B···C34B'' = 3.898(12) Å; (") $-x + 2, -y + 1, -z + 2$]. The reason for this difference in π – π stacking between the naphthyl groups of **2A** and those of **2B** is assumed to have to do with crystal packing interactions. Figure 4 shows the crystal packing view of **2** along the *a*-axis. The oxygen atom O7A of bridging nitrate in **2A** slightly overlapped at the gap between the naphthyl groups of **2B**. Due to this steric hindrance, it seems that the π – π stacking of the naphthyl groups was inhibited in **2B**. The crystal packing diagram for **2** is reported in Figure S4. As in the case of complex **1**, there is no evidence of a remarkable intermolecular interaction.

Similarly to **1**, in **2** the metal ions have octahedral coordination geometries. The axial bond distances between the nitrate oxygens and the Mn(III) ions, 2.244(6) Å for Mn1A–O5A and 2.261(6) Å for Mn1B–O5B, are ~0.1 Å longer than their counterparts measured in **1**. This evidence suggests that the magnetic exchange interaction between Mn(III) and Ni(II) in **2** might be smaller than corresponding parameter for **1**. Hetero-metal complexes with a *syn*–*syn* nitrate bridge are rare, with only a few examples reported in the literature [23]. To the best of our knowledge, complex **2** is the first example of a hetero-metal Mn^{III}Ni^{II} complex bridged by *syn*–*syn* nitrate anions. The coordination environment of Ni(II) in **2** is almost the same as that of the same metal ion in **1**, and the bond distances around Ni(II) are in the 1.976(5)–2.156(5) Å range. The average intramolecular metal-to-metal distances within **2A** and **2B** are 2.946(2) Å for Mn···Ni, 3.188(2) Å for Mn···Ni*, 3.188(3) Å for Ni···Ni*, and 5.246(3) Å for Mn···Mn*, respectively. The average bond angles around the μ_3 -alkoxo group are 92.9(2)° for Mn–O–Ni, 103.6(2)° for Mn–O–Ni*, and 98.0(2)° for Ni–O–Ni*. Given the substantial Mn···Ni* distance and the wide bond angles around the μ_3 -O center, the double-cubane core of **2** is distorted, but the distortion is rather small compared to the case of **1**.

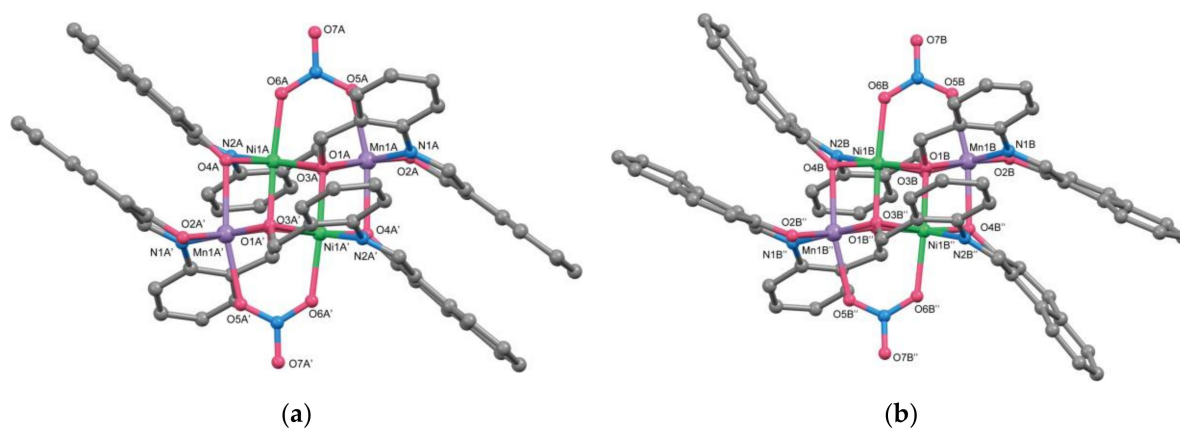


Figure 3. Perspective views of **2A** (a) and **2B** (b). Hydrogen atoms are omitted for clarity. Symmetry code: (') $-x + 2, -y, -z + 1$; (") $-x + 2, -y + 1, -z + 2$.

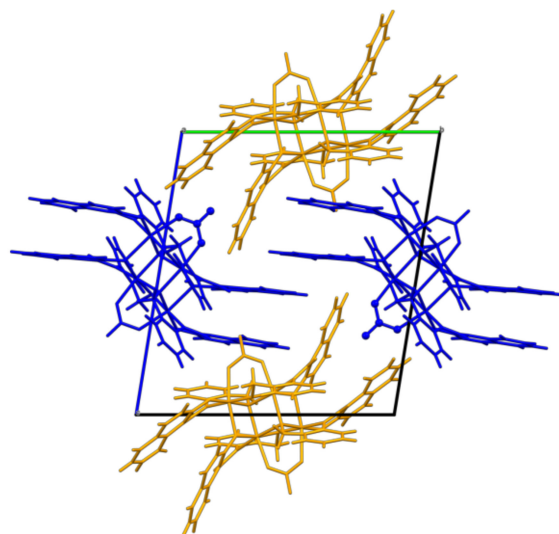


Figure 4. Packing view along the *a*-axis of **2**. Crystal solvents are omitted for clarity. Complex **2A** and **2B** are color coded with blue and orange, respectively.

2.3. Magnetic Property

Magnetic susceptibility measurements for **1** and **2** were performed with a SQUID (superconducting quantum interference device) magnetometer within the 4.5–300 K temperature range for **1** and the 2–300 K range for **2**. Figure 5 shows the temperature dependence of χ_m and $\chi_m T$ vs. *T* plots of **1** (a) and **2** (b).

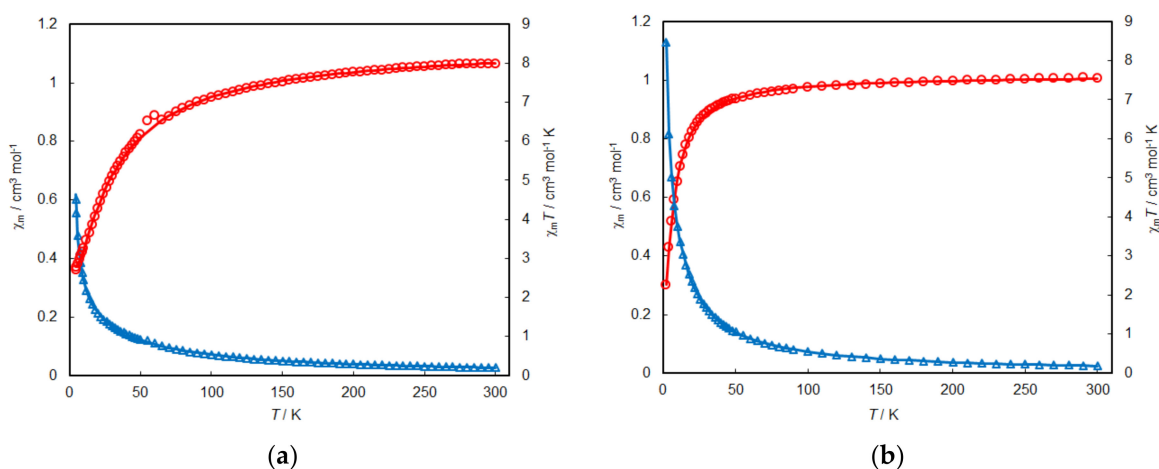


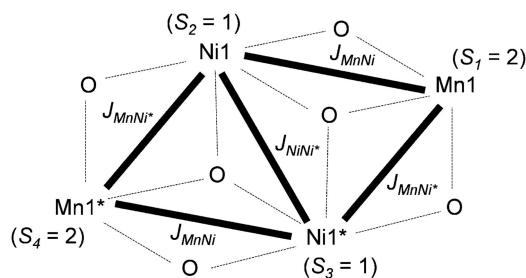
Figure 5. Temperature dependence of χ_m (blue triangles) and $\chi_m T$ (red circles) vs. *T* plots of **1** (a) and **2** (b). Solid lines are drawn with the best-fitted parameter values described in the text and in Table 2.

The $\chi_m T$ values at 300 K of **1** and **2** are, respectively, 7.98 and 7.55 $\text{cm}^3 \text{mol}^{-1} \text{K}$, which are slightly smaller than the spin-only value of 8.00 $\text{cm}^3 \text{mol}^{-1} \text{K}$ expected for magnetically uncoupled two high-spin Mn(III) ($S = 2$) and two Ni(II) ($S = 1$) system. With decreasing temperature, the $\chi_m T$ values for **1** gradually decrease to reach 2.71 $\text{cm}^3 \text{mol}^{-1} \text{K}$ at 4.5 K, which suggests an $S = 2$ ground state. This magnetic behavior closely resembles those previously reported for tetranuclear hetero-metal $\text{Mn}^{\text{III}}_2\text{Ni}^{\text{II}}_2$ complexes with bis- μ -alkoxo and *syn-syn* acetato triple bridges [24]. The $\chi_m T$ values for **2** are virtually constant from 300 K to 80 K; they then start decreasing as the temperature decreases below 80 K to reach 2.26 $\text{cm}^3 \text{mol}^{-1} \text{K}$ at 2.0 K. These magnetic behaviors indicate that for both **1** and

2 antiferromagnetic interactions are dominant in the hetero-metal tetranuclear cores. The magnetic analyses for **1** and **2** were simulated using the PHI program [25]. The Hamiltonian is written as:

$$\hat{H} = -2J_{MnNi}(\hat{S}_1\hat{S}_2 + \hat{S}_3\hat{S}_4) - 2J_{MnNi^*}(\hat{S}_1\hat{S}_3 + \hat{S}_2\hat{S}_4) - 2J_{MnMn^*}\hat{S}_1\hat{S}_4 - 2J_{NiNi^*}\hat{S}_2\hat{S}_3 + D_{Mn}(\hat{S}_1^2 + \hat{S}_4^2) + D_{Ni}(\hat{S}_2^2 + \hat{S}_3^2) \quad (1)$$

where J_{MnNi} is the exchange integral between the Mn and Ni ions in the asymmetric unit bridged by acetate or nitrate, whereas J_{MnNi^*} , J_{NiNi^*} , and J_{MnMn^*} are the exchange integrals between the metal ions located in the asymmetric units as defined in Scheme 1.



Scheme 1. Magnetic exchange coupling model for **1** and **2**.

In complexes **1** and **2**, the interaction J_{MnMn^*} can be ignored because the distance is too large to make a spin exchange [16,24]. The obtained J , g , and D parameters are the following: $J_{MnNi} = -4.19 \text{ cm}^{-1}$, $J_{MnNi^*} = -1.36 \text{ cm}^{-1}$, $J_{NiNi^*} = -4.03 \text{ cm}^{-1}$, $g_{Mn} = 2.14$, $g_{Ni} = 2.29$, $D_{Mn} = -0.22 \text{ cm}^{-1}$, and $D_{Ni} = 0.54 \text{ cm}^{-1}$ for **1**; $J_{MnNi} = -0.82 \text{ cm}^{-1}$, $J_{MnNi^*} = -0.66 \text{ cm}^{-1}$, $J_{NiNi^*} = 0.79 \text{ cm}^{-1}$, $g_{Mn} = 1.93$, $g_{Ni} = 2.01$, $D_{Mn} = -0.70 \text{ cm}^{-1}$, and $D_{Ni} = 0.37 \text{ cm}^{-1}$ for **2**. These results demonstrate that the magnetic interactions between Mn(III) and Ni(II) are antiferromagnetic in both complexes. In both cases, the absolute value $|J_{MnNi}|$ is larger than $|J_{MnNi^*}|$. The magnetic paths between Mn(III) and Ni(II) ions go through μ_2 -, μ_3 -alkoxo, and *syn-syn* acetato or nitrate bridges. Among them, the antiferromagnetic pathway through acetato bridges might be dominant. It is thought that the interaction J_{MnNi} influence most strongly the magnetic behavior of the complex. The interaction J_{MnNi} of **1** is much larger than its counterpart for **2**. As mentioned in Section 2.2, one of the reasons for this observation is that the metal–nitrate bonds in **2** are longer than the metal–acetate bonds in **1**. Results thus suggest that the acetato bridge is more effective than the nitrate bridge in assisting local spin-exchange interaction. The interactions J_{MnNi^*} , are relatively small due to the large bridging angles. The value of the metal–O–metal bridging angle is known to be one of the important parameters determining the magnitude of magnetic exchange interactions through phenoxo/hydroxo/alkoxo bridges. Typically, the cross-over angle in bridging 3d–3d systems lie in the 95–98° range [26,27]. The Mn–O–Ni* angles in **1** and **2** are large enough to assume the existence of antiferromagnetic interactions. For the interaction J_{NiNi^*} , the cross-over angle in dinickel(II) systems is 97.5° [28]. The Ni–O–Ni* angles in **1**, **2a**, and **2b** are 99.6(3), 98.0(2), and 98.0(2)°, respectively. The angle for **1** is larger than the cross-over angle known to afford an antiferromagnetic interaction. However, those for **2** are close to the mentioned value of 97.5°, leading to a weak ferromagnetic interaction. Hence, the difference in J_{NiNi^*} between **1** and **2** can be explained by the values of the Ni–O–Ni* angles.

Table 2. Best fitting magnetic parameters and μ_3 -O bridging angles of **1**, **2**, and related complexes.

Complex	J_{MnNi} (cm ⁻¹)	J_{MnNi^*} (cm ⁻¹)	J_{NiNi^*} (cm ⁻¹)	Mn–O–Ni (°)	Mn–O–Ni*(°)	Ni–O–Ni*(°)	References
Type-I: without <i>syn–syn</i> bridging ligand							
A	4.5	4.3	–7.9	97.3(2)	95.4(2)	101.6(2)	[12]
B	3.62	= J_{MnNi}	–7.81	98.51(14)	99.95(14)	97.85(14)	[24]
C	0.75	= J_{MnNi}	10	96.2(2)	99.3(2)	96.1(2)	[16]
Type-II: with <i>syn–syn</i> bridging carboxylate							
D	–1.80	= J_{MnNi}	–3.41	94.16(8)	103.61(8)	98.19(8)	[24]
E	–11.85	–6.44	0.34	95.7(1)	105.1(1)	100.4 ^{av}	[29]
1	–4.19	–1.36	–4.04	91.5(3)	106.1(3)	99.3(3)	This work
Type-III: with <i>syn–syn</i> bridging nitrate							
2	–0.82	–0.66	0.79	92.9(2) ^{av}	103.5(2) ^{av}	98.0(2) ^{av}	This work

A = [Mn^{III}₂Ni^{II}₂Cl₂(salpa)₂] (H₂salpa: *N*-(2-hydroxybenzyl)-3-amino-1-propanol); B = [Mn^{III}₂Ni^{II}₂(sap)₂(sal)₂(μ₃-OMe)₂(NO₃)₂(MeOH)₂] (H₂sap: *N*-(3-hydroxypropyl)salicylideneimine, Hsal: salicyl aldehyde); C = [Mn^{III}₂Ni^{II}₂Cl₂(L1)₄(H₂O)₂] (H₂L1: *N*-(2-hydroxy-methylphenyl)salicylideneimine); D = [Mn^{III}₂Ni^{II}₂(sap)₂(sal)₂(μ₃-OMe)₂(OAc)₂]; E = [Mn^{III}₂Ni^{II}₂(HL)₂L₂(OAc)₂(CH₃OH)₂] (H₂L: *N*-(2-hydroxy-5-fluoro-methylphenyl)-3-imine-2-propanol); av = an average angle in the asymmetric unit.

The J values and μ_3 -O bridging angles of structurally related tetranuclear Mn^{III}₂Ni^{II}₂ complexes are summarized in Table 2. Whether the overall magnetic behavior is ferromagnetic or antiferromagnetic is strongly influenced by the presence of *syn–syn* bridging ligands. The reported complexes without *syn–syn* bridging ligands (Type-I in Table 2) show totally ferromagnetic behavior, and in these complexes the Mn–O–Ni angles are in the 96–98° range. Those angles are nearly equal in size or smaller than the cross-over angle in phenoxo/alkoxo-bridged 3d–3d systems. In the case of complexes with *syn–syn* carboxylato bridges (Type-II), the Mn–O–Ni angles are much smaller than those of Type-I complexes. However, the bridging carboxylates provide a good magnetic exchange pathway. In addition, those complexes are characterized by a distortion of the double-cubane metal core that causes the large Mn–O–Ni* angles. These factors result in complexes **1** and **2** displaying antiferromagnetic properties. Finally, complex **2** is the first example of a Type-III complex, which is characterized by the presence of *syn–syn* nitrate bridges. Based on evidence gathered on other hetero-metal complexes [23], the magnetic pathway through the nitrate ligand is considered to have a small contribution to the magnetic exchange due to the weak coordination.

3. Materials and Methods

3.1. General

All chemicals were purchased and used as received, unless otherwise noted. Methanol was purified by distillation over magnesium turnings. The ligand H₂L was obtained by the literature method [13]. Elemental analyses for C, H, and N were obtained at the Elemental Analysis Service Center, Kyushu University. Analyses of Mn and Ni were made on a Shimadzu ICPS-8100 (Shimadzu Co. Ltd., Kyoto, Japan) twin sequential high-frequency plasma emission spectrometer. Fluorescent X-ray analyses were obtained on a Shimadzu Raynu EDX-700HS energy dispersive X-ray spectrometer (Shimadzu Co. Ltd., Kyoto, Japan). Infrared spectra were recorded on a Bruker VERTEX70-S FT-IR spectrometer on ATR (Attenuated Total Reflection) method at the Instrumental Analysis Center, Saga University. Reflection spectra were recorded on a PERKIN ELMER Lambda19 UV/VIS/NIR Spectrometer (PerkinElmer, Inc., Waltham, MA, USA) and Ocean Optics USB2000+ fiber optic spectrometer (Ocean Optics, Inc., Dunedin, FL, USA). The magnetic susceptibilities were measured on a Quantum Design MPMS-XL5R SQUID susceptometer (Quantum Design, Inc., San Diego, CA, USA) under an applied magnetic field of 0.5 T in the temperature range 2–300 K. The susceptibilities were corrected for the diamagnetism of the constituent atoms using Pascal’s constant [30].

3.2. Single Crystal X-ray Diffraction

X-ray diffraction measurements were made on a Rigaku AFC5S automated four-circle diffractometer (Rigaku Corp, Tokyo, Japan) for **1** and a Rigaku Vari-Max Saturn CCD 724 diffractometer (Rigaku Corp, Tokyo, Japan) for **2** with graphite monochromated Mo K α radiation ($\lambda = 0.71069$ Å).

Data were collected and processed using CrystalClear [31]. An empirical absorption correction was applied. The data were corrected for Lorentz and polarization effects. The crystal data and experimental parameters are summarized in Table S1. The structures were solved by direct methods (SIR92) and expanded using Fourier techniques [32,33]. The nonhydrogen atoms were refined anisotropically. All the hydrogen atoms, except those of the water molecule in **1** as crystal solvents which were not included in the structural models because their positions could not be determined precisely, were located on the calculated positions, and refined using the riding model. The final cycle of full-matrix least-squares refinement on F^2 using SHELXL-2016 [34] was based on observed reflections and variable parameters, and converged with unweighted and weighted agreement factors of R and R_w . All calculations were performed using the CrystalStructure [35] crystallographic software package of Molecular Structure Corporation except for refinement, which was performed using SHELXL-2016.

3.3. Synthesis of $[\text{Mn}_2\text{Ni}_2(\text{L})_4(\text{OAc})_2] \cdot \text{H}_2\text{O}$ (**1**)

A methanol solution (20 mL) of $\text{Mn}(\text{OAc})_3 \cdot 2\text{H}_2\text{O}$ (0.133 g, 0.5 mmol) and H_2L (0.278 g, 1.0 mmol) was added Et_3N (0.210 g, 2.0 mmol) drop-by-drop with stirring for 60 min. To the resulted solution was added a solution of $\text{NiCl}_2 \cdot 6\text{H}_2\text{O}$ (0.066 g, 0.5 mmol) in 5 mL methanol. After 60 min, brown precipitate was obtained. The brown single crystals were obtained by recrystallization of CH_2Cl_2 /toluene mixed solvent (9:1, 10 mL). $[\text{Mn}_2\text{Ni}_2(\text{L})_4(\text{OAc})_2] \cdot \text{H}_2\text{O}$; Yield: 17.8%. Anal. Calc. for $\text{C}_{76}\text{H}_{60}\text{Mn}_2\text{N}_4\text{Ni}_2\text{O}_{13}$: C, 62.30; H, 4.13; N, 3.83; Mn, 7.50; Ni, 8.01. Found: C, 62.02; H, 4.07; N, 3.85; Mn, 7.60; Ni, 7.92%. IR data $[\tilde{\nu}/\text{cm}^{-1}]$: 3060 (w), 2857 (w), 1615 (m), 1603 (m), 1572 (m), 1531 (s), 1376 (s), 1025 (m), 860 (s), 779 (s), 710 (m) and 566 (s). UV-VIS $[\tilde{\nu}/10^3 \text{ cm}^{-1}]$: 7.0^{sh}, 12^{sh}, 13^{sh}, 16^{sh}, 19^{sh}, 22^{sh} (sh = shoulder).

3.4. Synthesis of $[\text{Mn}_2\text{Ni}_2(\text{L})_4(\text{NO}_3)_2] \cdot 2\text{H}_2\text{O}$ (**2**)

A methanol solution (20 mL) of $\text{Mn}(\text{NO}_3)_2 \cdot 6\text{H}_2\text{O}$ (0.080 g, 0.278 mmol) and H_2L (0.278 g, 1.0 mmol) was added Et_3N (0.101 g, 1.00 mmol) drop-by-drop and refluxed for two hours. The mixture was added a methanol solution (5 mL) of $\text{Ni}(\text{NO}_3)_2 \cdot 6\text{H}_2\text{O}$ (0.073 g, 0.250 mmol) further refluxed for two hours. The resulting dark brown solution was evaporated to dryness under reduced pressure. The obtained oily substance was dissolved in 10 mL of CH_2Cl_2 including small amount of Na_2SO_4 with stirring. The dehydrated solution was filtered and left at room temperature. Dark brown crystals suitable for X-ray crystallography were obtained after two weeks. $[\text{Mn}_2\text{Ni}_2(\text{L})_4(\text{NO}_3)_2] \cdot 2\text{H}_2\text{O}$; Yield: 67.2%. Anal. Calc. for $\text{C}_{72}\text{H}_{56}\text{Mn}_2\text{N}_6\text{Ni}_2\text{O}_{16}$: C, 58.10; H, 3.79; N, 5.65; Mn, 7.38; Ni, 7.89. Found: C, 57.76; H, 3.61; N, 5.65; Mn, 7.02; Ni, 7.93%. IR data $[\tilde{\nu}/\text{cm}^{-1}]$: 3056 (w), 2926 (w), 2852 (w), 1619 (m), 1601 (m), 1575 (m), 1540 (s), 1436 (m), 1387 (s), 1361 (w), 1284 (m), 1030 (m), 829 (s), 758 (s), 654 (w) and 577 (m). UV-VIS $[\tilde{\nu}/10^3 \text{ cm}^{-1}]$: 12^{sh}, 13^{sh}, 16^{sh}, 19^{sh}, 22^{sh}.

4. Conclusions

New tetranuclear hetero-metal $\text{Mn}^{\text{III}}_2\text{Ni}^{\text{II}}_2$ complexes, $[\text{Mn}_2\text{Ni}_2(\text{L})_4(\text{OAc})_2]$ and $[\text{Mn}_2\text{Ni}_2(\text{L})_4(\text{NO}_3)_2]$, were prepared by the simple one-pot reaction of metal sources with Schiff base ligand. Single crystal X-ray analyses reveal that these complexes adopt defective double-cubane metal cores with *syn-syn* bridging acetate or nitrate. The temperature dependent magnetic susceptibility measurements showed that both complexes have antiferromagnetic behaviors and $S = 2$ ground state. The obtained magnetic parameters indicate that all magnetic pathway in the hetero-metal core are weak antiferromagnetic.

Supplementary Materials: The following are available online at <http://www.mdpi.com/2312-7481/5/1/14/s1>, Figure S1. IR spectrum of **1** (ATR). Figure S2. IR spectrum of **2** (ATR). Figure S3. Molecular packing diagram of **1**. Figure S4. Molecular packing diagram of **2**. Table S1. Crystallographic data of **1** and **2**. Table S2. Bond angles in the coordination spheres of **1**, **2A**, and **2B**.

Author Contributions: Conceptualization: M.K. and T.T.; syntheses: R.M. and T.T.; crystallographic measurements and characterization: R.M., Y.Y., and M.K.; spectroscopic measurements: Y.S., R.M. and T.T.; magnetic measurements: M.M.; magnetic analyses: Y.S.; writing—original draft preparation: Y.S.; writing—review and editing: M.K.; project administration: M.K.; funding acquisition: M.K.

Funding: This research was partially supported by JSPS KAKENHI Grant Number JP23550080 and 26410075 from Japan Society for the Promotion of Science.

Conflicts of Interest: The authors declare no conflicts of interest.

References

1. Ma, X.-F.; Wang, Z.; Chen, X.-L.; Kurmoo, M.; Zeng, M.-H. Ligand effect on the single-molecule magnetism of tetranuclear Co(II) cubane. *Inorg. Chem.* **2017**, *56*, 15178–15186. [[CrossRef](#)] [[PubMed](#)]
2. Das, S.; Dey, A.; Biswas, S.; Calacio, E.; Chandrasekhar, V. Hydroxide-free cubane-shaped tetranuclear [Ln₄] complexes. *Inorg. Chem.* **2014**, *53*, 3417–3426. [[CrossRef](#)]
3. Nayak, S.; Aromi, G.; Teat, S.J.; Ribas-Ariño, J.; Gamez, P.; Reedijk, J. Hydrogen bond assisted co-crystallization of a bimetallic Mn^{III}₂Ni^{II}₂ cluster and a Ni^{II}₂ cluster unit: Synthesis, structure, spectroscopy and magnetism. *Dalton Trans.* **2010**, *39*, 4986–4990. [[CrossRef](#)] [[PubMed](#)]
4. Oshio, H.; Hoshino, N.; Ito, T.; Nakano, M. Single-molecule of ferrous cubes: Structurally controlled magnetic anisotropy. *J. Am. Chem. Soc.* **2004**, *126*, 8805–8812. [[CrossRef](#)]
5. Mahapatra, P.; Drew, G.B.M.; Ghosh, A. Ni(II) Complex of N₂O₃ donor unsymmetrical ligand and its use for the synthesis of Ni^{II}–Mn^{II} complexes of diverse nuclearity: Structures, magnetic properties, and catalytic oxidase activities. *Inorg. Chem.* **2018**, *57*, 8338–8353. [[CrossRef](#)] [[PubMed](#)]
6. Marino, N.; Armentano, D.; Mastropietro, T.F.; Julve, M.; Munno, G.D.; Martínez-Lillo, J. Cubane-type Cu^{II}₄ and Mn^{II}₂Mn^{III}₂ complexes based on pyridoxine: A versatile ligand for metal assembling. *Inorg. Chem.* **2013**, *52*, 11934–11943. [[CrossRef](#)] [[PubMed](#)]
7. Wang, H.-S.; Song, Y. Conversion of tetranuclear Ni complexes from a defect dicubane core to a [Ni₄O₄] cubane-like core via addition of 2-hydroxymethylpyridine: Synthesis, crystal structures, and magnetic properties. *Inorg. Chem. Comm.* **2013**, *35*, 86–88. [[CrossRef](#)]
8. Nayak, S.; Novitchi, G.; Muche, S.; Luneau, D.; Dehnen, S. Tetranuclear homo- and heterometallic manganese(III) and nickel(II) complexes: Synthesis, structure, and magnetic studies. *Zeitschrift für Anorganische und Allgemeine Chemie* **2012**, *638*, 1127–1133. [[CrossRef](#)]
9. Brechin, E.K.; Soler, M.; Christou, G.; Davidson, J.; Hendrickson, D.N.; Parson, S.; Wernsdorfer, W. Magnetization tunneling in an enneanuclear manganese cage. *Polyhedron* **2003**, *22*, 1771–1775. [[CrossRef](#)]
10. Nakajima, T.; Seto, K.; Scheurer, A.; Kure, B.; Kajiwara, T.; Tanase, T.; Mikuriya, M.; Sakiyama, H. Tetranuclear nickel and cobalt complexes with an incomplete double-cubane structure—Homo- and heterometallic complexes and their 1D coordination polymers. *Eur. J. Inorg. Chem.* **2014**, 5021–5033. [[CrossRef](#)]
11. Yamashita, H.; Koikawa, M.; Tokii, T. Synthesis, structure, and magnetic properties of tetranuclear copper(II) complexes of tridentate dianionic ligands with an ONO donor set. *Mol. Cryst. Liq. Cryst.* **2000**, *342*, 63–68. [[CrossRef](#)]
12. Oshio, H.; Nihei, M.; Koizumi, S.; Shiga, T.; Nojiri, H.; Nakano, M.; Shirakawa, N.; Akatsu, M. A heterometal single-molecule magnet of [Mn^{III}₂Ni^{II}₂Cl₂(salpa)₂]. *J. Am. Chem. Soc.* **2005**, *127*, 4568–4569. [[CrossRef](#)] [[PubMed](#)]
13. Modak, R.; Sikdar, Y.; Thuijs, A.E.; Christou, G.; Goswami, S. Co^{II}₄, Co^{II}₇, and a series of Co^{II}₂Ln^{III} (Ln^{III} = Nd^{III}, Sm^{III}, Gd^{III}, Tb^{III}, Dy^{III}) coordination clusters: Search for single molecule magnets. *Inorg. Chem.* **2016**, *55*, 10192–10202. [[CrossRef](#)]
14. Nath, M.; Yadav, R. Synthesis, spectral and thermal studies of Fe(III), Co(II), Ni(II), Cu(II) and Zn(II) complexes of Schiff bases derived from *o*-aminobenzyl alcohol. *Synth. React. Inorg. Met. Org. Chem.* **1995**, *25*, 1529–1547. [[CrossRef](#)]
15. Koikawa, M.; Yamashita, H.; Tokii, T. Crystal structures and magnetic properties of tetranuclear copper(II) complexes of *N*-(2-hydroxymethylphenyl)salicylideneimine with a defective double-cubane core. *Inorg. Chim. Acta* **2004**, *357*, 2635–2642. [[CrossRef](#)]
16. Koikawa, M.; Ohba, M.; Tokii, T. Syntheses, structures, and magnetic properties of tetranuclear Ni^{II}₄ and Ni^{II}₂Mn^{III}₂ complexes with ONO tridentate ligands. *Polyhedron* **2005**, *24*, 2257–2262. [[CrossRef](#)]

17. Yoshitake, M.; Nishihashi, M.; Ogata, Y.; Yoneda, K.; Yamada, Y.; Sakiyama, H.; Mishima, A.; Ohba, M.; Koikawa, M. Syntheses, structures, and magnetic properties of cubane-based cobalt and nickel complexes with ONO-tridentate ligands. *Polyhedron* **2017**, *136*, 136–142. [CrossRef]
18. Brown, I.D. *The Chemical Bond in Inorganic Chemistry: The Bond Valence Model*, 2nd ed.; Oxford University Press: Oxford, UK, 2002; ISBN 9780198742951.
19. Brown, I.D. Accumulated Table of Bond Valence Parameters. 2016. Available online: <http://www.iucr.org/resources/data/datasets/bond-valence-parameters/> (accessed on 18 March 2016).
20. Modak, R.; Sikdar, Y.; Mandal, S.; Gómez-García, C.J.; Benmansour, S.; Chatterjee, S.; Goswami, S. Homo and heterometallic rhomb-like Ni₄ and Mn₂Ni₂ complexes. *Polyhedron* **2014**, *70*, 155–163. [CrossRef]
21. Daier, V.; Biava, H.; Palopoli, C.; Shova, S.; Tuchagues, J.-P.; Signorella, S. Synthesis, characterization and catalase-like activity of dimanganese(III) complexes of 1,5-bis(5-X-salicylidenamino)pentan-3-ol (X = nitro and chloro). *J. Inorg. Biochem.* **2004**, *98*, 1806–1817. [CrossRef] [PubMed]
22. Yoshitake, M.; Yoneda, K.; Yamada, Y.; Koikawa, M. Synthesis and crystal structure of a tetranuclear Mn(III)-Ni(II) heterometal complex of N-(2-oxymethylphenyl)salicylideneimine. *X-ray Struct. Anal. Online* **2016**, *32*, 1–2. [CrossRef]
23. Colacio, E.; Ruiz-Sanchez, J.; White, F.J.; Brechin, E.K. Strategy for the rational design of asymmetric triply bridged dinuclear 3d-4f single-molecule magnets. *Inorg. Chem.* **2011**, *50*, 7268–7273. [CrossRef]
24. Nihei, M.; Yoshida, A.; Koizumi, S.; Oshio, H. Hetero-metal Mn–Cu and Mn–Ni clusters with tridentate Schiff-base ligands. *Polyhedron* **2007**, *26*, 1997–2007. [CrossRef]
25. Chilton, N.F.; Anderson, R.P.; Turner, L.D.; Soncini, A.; Murray, K.S. PHI: A powerful new program for the analysis of anisotropic monomeric and exchange-coupled polynuclear *d*- and *f*-block complexes. *J. Comput. Chem.* **2013**, *34*, 1164–1175. [CrossRef] [PubMed]
26. Kahn, O. *Molecular Magnetism*; VCH Publications: New York, NY, USA, 1993; pp. 145–210, ISBN 1-56081-566-3.
27. Sasmal, S.; Roy, S.; Carrella, L.; Jana, A.; Rentschler, E.; Mohanta, S. Structures and magnetic properties of bis(μ-phenoxido), bis(μ-phenoxido)-μ-carboxylato and bis(μ-phenoxido)bis(μ-carboxylato) Fe^{III}Ni^{II} compounds—Magnetostructural correlations. *Eur. J. Inorg. Chem.* **2015**, 680–689. [CrossRef]
28. Nanda, K.K.; Thompson, L.K.; Bridson, J.N.; Nag, K. Linear dependence of spin exchange coupling constant on bridge angle in phenoxy-bridged dinickel(II) complexes. *J. Chem. Soc. Chem. Commun.* **1994**, 1337–1338. [CrossRef]
29. Ding, Y.; Xu, J.; Pan, Z.; Zhou, H.; Lou, X. Structure, magnetic property and DNA cleavage ability of heterometal Mn^{III}₂Ni^{II}₂ complex with ONO tridentate ligands *Inorg. Chem. Comm.* **2012**, *22*, 40–43. [CrossRef]
30. Selwood, P.W. *Magnetochemistry*; Interscience Publishers: New York, NY, USA, 1956; pp. 78–91.
31. Rigaku Corporation. *CrystalClear: Data Collection and Processing Software*; Rigaku Corporation: Tokyo, Japan, 1998.
32. Altomare, A.; Cascarano, G.; Giacovazzo, C.; Guagliardi, A. Completion and refinement of crystal structures with SIR92. *J. Appl. Cryst.* **1993**, *26*, 343–350. [CrossRef]
33. Beurskens, P.T.; Admiraal, G.; Beurskens, G.; Bosman, W.P.; Gelder, R.; Israel, R.; Smits, J.M.M. DIRDIF99. Master's Thesis, Crystallography Laboratory University of Nijmegen, Nijmegen, The Netherlands, 1999.
34. Sheldrick, G.M. Crystal structure refinement with SHELXL. *Acta Crystallogr.* **2015**, *C71*, 3–8. [CrossRef]
35. Rigaku Corporation. *CrystalStructure: Crystal Structure Analysis Package (Version 4.3)*; Rigaku Corporation: Tokyo, Japan, 2000.

